Proc. Natl. Acad. Sci. USA
Vol. 94, pp. 12366–12371, November 1997
Biophysics

Attenuated T_2 relaxation by mutual cancellation of dipole–dipole coupling and chemical shift anisotropy indicates an avenue to NMR structures of very large biological macromolecules in solution

KONSTANTIN PERVUSHIN, ROLAND RIEK, GERHARD WIDER, AND KURT WÜTHRICH*

Institut für Molekularbiologie und Biophysik Eidgenössische Technische Hochschule Hönggerberg CH-8093 Zurich, Switzerland

Contributed by Kurt Wüthrich, September 3, 1997

ABSTRACT **Fast transverse relaxation of ^{1}H, ^{15}N, and ^{13}C by dipole-dipole coupling (DD) and chemical shift anisotropy (CSA) modulated by rotational molecular motions has a dominant impact on the size limit for biomacromolecular structures that can be studied by NMR spectroscopy in solution. Transverse relaxation-optimized spectroscopy (TROSY) is an approach for suppression of transverse relaxation in multidimensional NMR experiments, which is based on constructive use of interference between DD coupling and CSA. For example, a TROSY-type two-dimensional ^{1}H,^{15}N-correlation experiment with a uniformly ^{15}N-labeled protein in a DNA complex of molecular mass 17 kDa at a ^{1}H frequency of 750 MHz showed that ^{15}N relaxation during ^{15}N chemical shift evolution and $^1H^N$ relaxation during signal acquisition both are significantly reduced by mutual compensation of the DD and CSA interactions. The reduction of the linewidths when compared with a conventional two-dimensional ^{1}H,^{15}N-correlation experiment was 60% and 40%, respectively, and the residual linewidths were 5 Hz for ^{15}N and 15 Hz for $^1H^N$ at 4°C. Because the ratio of the DD and CSA relaxation rates is nearly independent of the molecular size, a similar percentagewise reduction of the overall transverse relaxation rates is expected for larger proteins. For a ^{15}N-labeled protein of 150 kDa at 750 MHz and 20°C one predicts residual linewidths of 10 Hz for ^{15}N and 45 Hz for $^1H^N$, and for the corresponding uniformly ^{15}N,^{2}H-labeled protein the residual linewidths are predicted to be smaller than 5 Hz and 15 Hz, respectively. The TROSY principle should benefit a variety of multidimensional solution NMR experiments, especially with future use of yet somewhat higher polarizing magnetic fields than are presently available, and thus largely eliminate one of the key factors that limit work with larger molecules.**

NMR spectroscopy with proteins based on observation of a small number of spins with outstanding spectral properties, which either may be present naturally or introduced by techniques such as site-specific isotope labeling, yielded biologically relevant information on human hemoglobin (M = 65,000) as early as 1969 (1), and subsequently also for significantly larger systems such as Igs (2). In contrast, the use of NMR for *de novo* structure determination (3, 4) so far has been limited to relatively small molecular sizes, with the largest NMR structure below molecular weight 30,000. Although NMR in structural biology may, for practical reasons of coordinated use with x-ray crystallography (5), focus on smaller molecular sizes also in the future, considerable effort goes into attempts to extend the size limit to bigger molecules (for example, see refs. 6–8). Here we introduce transverse relaxation-optimized spectroscopy (TROSY) and present experimental data and theoretical considerations showing that this approach is capable of significantly reducing transverse relaxation rates and thus overcomes a key obstacle opposing solution NMR of larger molecules (7).

At the high magnetic fields typically used for studies of proteins and nucleic acids, chemical shift anisotropy interaction (CSA) of ^{1}H, ^{15}N, and ^{13}C nuclei forms a significant source of relaxation in proteins and nucleic acids, in addition to dipole–dipole (DD) relaxation. This leads to increase of the overall transverse relaxation rates with increasing polarizing magnetic field, B_0. Nonetheless, transverse relaxation of amide protons in larger proteins at high fields has been reduced successfully by complete or partial replacement of the nonlabile hydrogen atoms with deuterons and, for example, more than 90% of the ^{15}N, $^{13}C^{\alpha}$, and $^1H^N$ chemical shifts thus were assigned in the polypeptide chains of a protein-DNA complex of size 64,000 (6). TROSY uses spectroscopic means to further reduce T_2 relaxation based on the fact that cross-correlated relaxation caused by DD and CSA interference gives rise to different relaxation rates of the individual multiplet components in a system of two coupled spins ½, I and S, such as the ^{15}N–^{1}H fragment of a peptide bond (9, 10). Theory shows that at ^{1}H frequencies near 1 GHz nearly complete cancellation of all transverse relaxation effects within a ^{15}N–^{1}H moiety can be achieved for one of the four multiplet components. TROSY observes exclusively this narrow component, for which the residual linewidth is then almost entirely because of DD interactions with remote hydrogen atoms in the protein. These can be efficiently suppressed by ^{2}H-labeling, so that in TROSY-type experiments the accessible molecular size for solution NMR studies no longer is primarily limited by T_2 relaxation.

Theory

We consider a system of two scalar coupled spins ½, I and S, with a scalar coupling constant J_{IS}, which is located in a protein molecule. T_2 relaxation of this spin system is dominated by the DD coupling of I and S and by CSA of each individual spin, because the stereochemistry of the polypeptide chain restricts additional interactions of I and S to weak scalar and DD couplings with a small number of remote protons, I_k. The relaxation rates of the individual multiplet components of spin S in a single quantum spectrum then may be widely different (9, 11, 12). They can be described by using the single-transition basis operators $S^{\pm}_{34}$ and $S^{\pm}_{12}$ (13), which refer to the transitions 1→2 and 3→4 in the standard energy-level diagram for a

The publication costs of this article were defrayed in part by page charge payment. This article must therefore be hereby marked "*advertisement*" in accordance with 18 U.S.C. §1734 solely to indicate this fact.

Abbreviations: rf, radio frequency; DD, dipole–dipole; CSA, chemical shift anisotropy; COSY, correlation spectroscopy; TROSY, transverse relaxation-optimized spectroscopy; *ftz* homeodomain, *fushi tarazu* homeodomain polypeptide of 70 amino acid residues, with the homeodomain in positions 3–62.

*To whom reprint requests should be addressed.

system of two spins ½, and are associated with the corresponding resonance frequencies, $\omega_S^{12} = \omega_S + \pi J_{IS}$ and $\omega_S^{34} = \omega_S - \pi J_{IS}$ (13–16):

$$\frac{d}{dt}\begin{bmatrix} \langle S_{12}^{\pm}\rangle \\ \langle S_{34}^{\pm}\rangle \end{bmatrix} = -\begin{bmatrix} \pm i\omega_S^{12} + R_{1212} + \frac{1}{T_{2S}} + \frac{1}{2T_{1I}} & 3(p^2 - \delta_I^2)J(\omega_I) - \frac{1}{2T_{1I}} \\ 3(p^2 - \delta_I^2)J(\omega_I) - \frac{1}{2T_{1I}} & \pm i\omega_S^{34} + R_{3434} + \frac{1}{T_{2S}} + \frac{1}{2T_{1I}} \end{bmatrix} \cdot \begin{bmatrix} \langle S_{12}^{\pm}\rangle \\ \langle S_{34}^{\pm}\rangle \end{bmatrix}. \quad [1]$$

ω_S and ω_I are the Larmor frequencies of the spins S and I, T_{2S} and T_{1I} account for the transverse relaxation of spin S and the longitudinal relaxation time of spin I, respectively, by all mechanisms of relaxation except DD coupling between the spins S and I and CSA of the spins S and I.

$$p = \frac{1}{2\sqrt{2}}\gamma_I\gamma_S\hbar/r_{IS}^3,\ \delta_S = \frac{1}{3\sqrt{2}}\gamma_S B_0 \Delta\sigma_S$$

and

$$\delta_I = \frac{1}{3\sqrt{2}}\gamma_I B_0 \Delta\sigma_I,$$

where γ_I and γ_S are the gyromagnetic ratios of I and S, $\hbar$ is the Planck constant divided by 2π, r_{IS} the distance between S and I, B_0 the polarizing magnetic field, and $\Delta\sigma_S$ and $\Delta\sigma_I$ are the differences between the axial and the perpendicular principal components of the axially symmetric chemical shift tensors of spins S and I, respectively. R_{1212} and R_{3434} are the transverse relaxation rates of the individual components of the S doublet (11) given by Eqs. **2** and **3**,

$$R_{1212} = (p - \delta_S)^2(4J(0) + 3J(\omega_S)) + p^2(J(\omega_I - \omega_S) + 3J(\omega_I) + 6J(\omega_I + \omega_S)) + 3\delta_I^2 J(\omega_I), \quad [2]$$

$$R_{3434} = (p + \delta_S)^2(4J(0) + 3J(\omega_S)) + p^2(J(\omega_I - \omega_S) + 3J(\omega_I) + 6J(\omega_I + \omega_S)) + 3\delta_I^2 J(\omega_I), \quad [3]$$

where $J(\omega)$ represents the spectral density functions at the frequencies indicated:

$$J(\omega) = \frac{2\tau_c}{5(1 + (\tau_c\omega)^2)}. \quad [4]$$

In deriving Eqs. **2** and **3**, parallel orientation of the principal symmetry axis of the chemical shift tensor and the vector $\mathbf{r}_{IS}$ was assumed. These equations show that whenever CSA and DD coupling are comparable, i.e. $p \approx \delta_S$, the resonance at frequency ω_S^{12} may exhibit slow transverse relaxation even for very large molecules.

For a treatment of the relaxation of spin I by Eq. **1** the symbols I and S simply can be interchanged. The single-transition operators $I_{13}^{\pm}$ and $I_{24}^{\pm}$ then refer to the transitions between the energy levels 1→3 and 2→4, respectively, which are associated with the frequencies $\omega_I^{13} = \omega_I + \pi J_{IS}$ and $\omega_I^{24} = \omega_I - \pi J_{IS}$, and the relaxation rates R_{1313} and R_{2424} are determined by equations obtained by permutation of the S and I indices in Eqs. **2** and **3**, respectively.

To evaluate the contributions from other mechanisms of relaxation we identify I and S as the $^1H^N$ and ^{15}N spins in a ^{15}N–^1H moiety. The relaxation of ^{15}N then is mainly determined by the CSA of ^{15}N and the DD interactions with the directly attached proton (17), so that the contributions from other interactions, $1/T_{1S}$ and $1/T_{2S}$, to a good approximation can be neglected. For $^1H^N$, $1/T_{1I}$ and $1/T_{2I}$ are dominated by DD interactions with other protons I_k at distance r_k. These can be accounted for by spectral density functions $J_k(\omega)$, which describe the motions of the vectors joining the individual $^1H^N$–^1H_k spin pairs (17):

$$1/T_{1I} = \sum_k (\gamma_I^2\hbar/2r_k^3)^2(J_k(0) + 3J_k(\omega_I) + 6J_k(2\omega_I)), \quad [5]$$

$$1/T_{2I} = \sum_k (\gamma_I^2\hbar/2r_k^3)^2\left(\frac{5}{2}J_k(0) + \frac{9}{2}J_k(\omega_I) + 3J_k(2\omega_I)\right). \quad [6]$$

Here, Eqs. **1**-**6** were used to calculate theoretical lineshapes of spin multiplets for given sets of the relaxation parameters, which subsequently were compared with the experimental NMR data. In particular, the in-phase absorptive spectrum was calculated using Eq. **7** (14),

$$I(\omega) = \mathrm{Re}[\mathbf{V}\mathbf{A}^{-1}\mathbf{V}^T], \quad \mathbf{A} = \boldsymbol{M} - i\omega\boldsymbol{E}, \quad [7]$$

where $\mathbf{V} = (1,1)$, and the relaxation matrix $\mathbf{A}$ is the (2×2) matrix on the right side of Eq. **1**, and $\boldsymbol{E}$ is the unity matrix.

Experimental Procedures

NMR spectra were recorded on Bruker DRX 750 and Varian Unity*plus* 400 spectrometers with a 2 mM solution of the specific 1:1 complex formed between a uniformly ^{15}N-labeled 70-residue *fushi tarazu (ftz)* homeodomain polypeptide and an unlabeled 14-bp DNA duplex (18, 19) in 95% ^1H_2O/5% ^2H_2O at pH 6.0 and 4°C.

The isotropic rotational correlation time, τ_c, of the complex was estimated from the T_1/T_2 ratio of the relaxation times of the backbone ^{15}N nuclei (20). The experimental schemes of

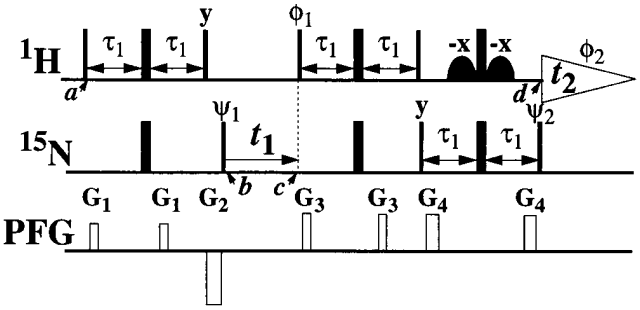

FIG. 1. Experimental scheme for TROSY-type two-dimensional ^1H,^{15}N correlation spectroscopy. In the rows marked ^1H and ^{15}N, narrow and wide bars stand for nonselective 90° and 180° rf-pulses, respectively. Water suppression is achieved by WATERGATE (34), using the two off-resonance rf-pulses indicated by curved shapes. The ^1H and ^{15}N carrier frequencies are placed at 9 and 127 ppm, respectively. The delay τ_1 corresponds to $1/(4^1J(^1H,^{15}N)) = 2.7$ ms. Phases used are $\psi_1 = \{y,-y,-x,x,y,-y,-x,x\}$; $\psi_2 = \{4(x),4(-x)\}$; $\phi_1 = \{4(y),4(-y)\}$; ϕ_2 (receiver) $= \{x,-x,-y,y,x,-x,y,-y\}$; x on all other pulses. The row marked PFG (pulsed field gradient) indicates the applied magnetic field gradients along the z-axis: G_1, amplitude = 30 G/cm, duration = 0.4 ms; G_2, −60 G/cm, 1 ms; G_3, 50 G/cm, 0.4 ms; G_4, 48 G/cm, 0.6 ms. Two free induction decays are recorded per t_1 delay, with ψ_1 incremented by 90° in between and stored as the real and imaginary parts of the interferogram in t_1. The Fourier transformation results in a two-dimensional ^1H,^{15}N correlation spectrum that contains only the component of the four-line ^{15}N–^1H multiplet that has the slowest T_2 relaxation rates for both nuclei. With this scheme, DD/CSA relaxation interference, which has been known for many years (35, 36), can be used to extend the limits of protein NMR.

Farrow *et al.* (21) were used for measurements of T_1 (^{15}N) and T_2 (^{15}N) for backbone nitrogen atoms.

The TROSY approach (Fig. 1) and conventional [^{15}N,^{1}H]correlation spectroscopy (COSY) (22, 23) experiments were used to correlate ^{1}H and ^{15}N resonances. For all spectra t_{1max} = 90 ms and t_{2max} = 171 ms were used. In TROSY the evolution of the *I,S* spin system due to the $^{1}J_{IS}$ scalar coupling was not refocused during t_1 and t_2, thus avoiding suppression of cross-correlated relaxation during these periods. To obtain the pure absorptive spectrum containing only the most slowly relaxing component of the two-dimensional multiplets, the scheme of Fig. 1 was used (see also *Appendix: Quantitative Analysis of TROSY*).

Results

The NMR experiments with the uniformly ^{15}N-labeled *ftz* homeodomain complexed with a 14-bp DNA duplex were performed at 4°C. The T_1/T_2 ratio of ^{15}N was used to estimate the effective global correlation time, τ_c, of the complex (20). For the backbone amide groups, average T_1 (^{15}N) and T_2 (^{15}N) values of 0.720 ± 0.03 and 0.042 ± 0.005 s, respectively, were measured at 400 MHz, resulting in a global rotational correlation time of τ_c = 20 ± 2 ns. This τ_c value corresponds to that expected for a spherical protein of size 40 kDa in H_2O solution at 35°C.

Fig. 2 shows a small region from ^{15}N–^{1}H correlation spectra of the *ftz* homeodomain-DNA complex that contains the resonance of the indole ^{15}N–^{1}H moiety of Trp-48, which is buried in the core of the protein (19). In the conventional [^{15}N,^{1}H]COSY experiment (22, 23), decoupling of ^{1}H and ^{15}N during the time periods t_1 and t_2, respectively, leads to detection of a single correlation peak per ^{15}N–^{1}H moiety (Fig. 2*a*). If the same [^{15}N,^{1}H]COSY spectrum is recorded without decoupling, four cross-peaks are observed per ^{15}N–^{1}H moiety, which show largely different linewidths (Fig. 2*b*). The cross-peak at (ω_1 = 130.7 ppm, ω_2 = 10.78 ppm) exhibits the broadest linewidths in both dimensions, which shows that it originates from the rapidly relaxing components of both $^{1}H^{N}$ and ^{15}N. One-dimensional cross-sections taken along ω_2 and ω_1 at the positions indicated by arrows in the spectra presented in Fig. 2 show that the two cross-peaks at (ω_1 = 132.1 ppm, ω_2 = 10.78 ppm) and (ω_1 = 130.7 ppm, ω_2 = 10.65 ppm) are broadened either along ω_1 or along ω_2 (Fig. 3). The cross-peak at (ω_1 = 132.1 ppm, ω_2 = 10.65 ppm) displays narrow linewidths in both dimensions, showing that it originates from the two slowly relaxing components of the ^{15}N–^{1}H doublets. The TROSY-type correlation experiment, which does not use decoupling either during t_1 or t_2, contains only this narrowest correlation peak (Fig. 2*c*), which shows about 60% and 40% decrease in the linewidths of the ^{15}N and ^{1}H resonances, respectively, when compared with the collapsed cross-peak in the conventional, broadband-decoupled spectrum (Fig. 2).

The fits of the experimental line shapes shown in Fig. 3 were obtained with line-shape calculations using the parameters τ_c = 20 ns and $^{1}J(^{1}H,^{15}N)$ = 105 Hz, where the chemical shift anisotropies, $\Delta\sigma_H$ and $\Delta\sigma_N$, were adjusted for the best fit. Because there was an otherwise unaccountable deviation from the Lorentzian lineshape we included a long-range scalar coupling $^{2}J(^{1}H^{\delta1},^{15}N^{\varepsilon1})$ = −5 Hz (24) in the calculations, and T_1 and T_2 relaxation of $^{1}H^{N}$ because of DD coupling with other protons was modeled by placing three protons at a distance of 0.24 nm from $^{1}H^{N}$. Application of one or a series of 180° pulses on spin *I* during the evolution of spin *S* interchanges the slowly and rapidly relaxing components of the *S* multiplet, which results in averaging of the slow and fast relaxation rates and elimination of the CSA/DD interference (25, 26). Indeed, the line shapes of the $^{1}H^{N}$ and ^{15}N resonances measured with conventional [^{15}N,^{1}H]COSY are well reproduced if the average of the two relaxation rates is used in the simulation (Fig. 3 *a1* and *b1*). The best-fit values of

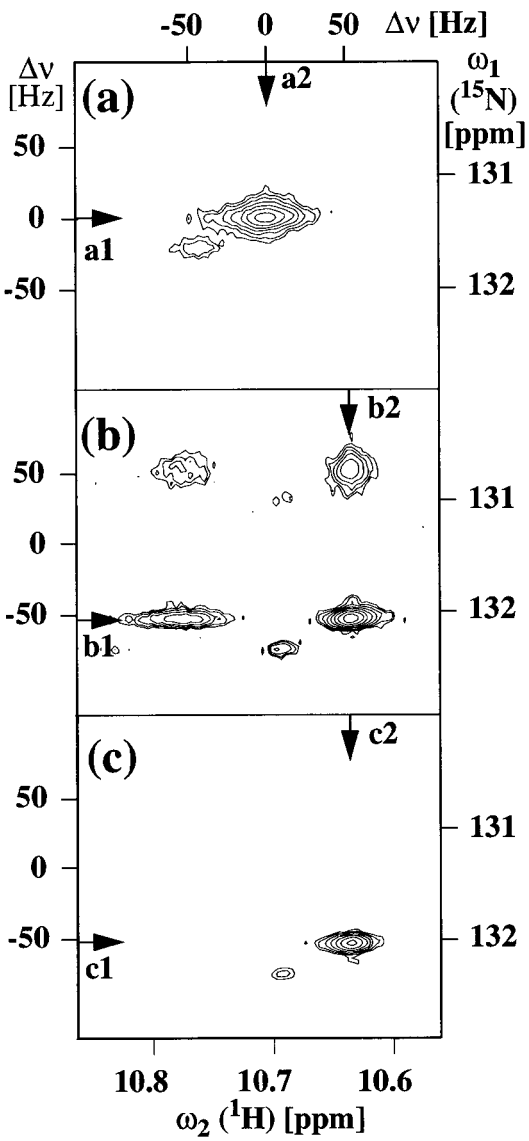

FIG. 2. Contour plots of ^{15}N,^{1}H correlation spectra showing the indole ^{15}N–^{1}H spin system of Trp-48 recorded in a 2 mM solution of uniformly ^{15}N-labeled *ftz* homeodomain complexed with an unlabeled 14-bp DNA duplex in 95% H_2O/5% $^{2}H_2O$ at 4°C, pH = 6.0, measured at the ^{1}H frequency of 750 MHz. (*a*) Conventional broad-band decoupled [^{15}N,^{1}H]COSY spectrum (22, 23). The evolution caused by the $^{1}J(^{1}H,^{15}N)$ scalar coupling was refocused in the ω_1 and ω_2 dimensions by a 180° proton pulse in the middle of the ^{15}N evolution time t_1, and by WALTZ composite pulse decoupling of ^{15}N during data acquisition, respectively. (*b*) Conventional [^{15}N,^{1}H]COSY spectrum recorded without decoupling during t_1 and t_2. (*c*) TROSY-type ^{15}N,^{1}H correlation spectrum recorded with the pulse scheme of Fig. 1. Chemical shifts relative to DSS in ppm and shifts in Hz relative to the center of the multiplet are indicated in both dimensions. The arrows identify the locations of the cross-sections shown in Fig. 3.

$\Delta\sigma_H$ = −16 ppm and $\Delta\sigma_N$ = −160 ppm correspond closely to the experimentally measured chemical shift anisotropies of ^{1}H and ^{15}N in ^{15}N–^{1}H moieties. With solid-state NMR studies of ^{15}N–^{2}D moieties, values for $\Delta\sigma_D$ near −14 ppm (27) and for $\Delta\sigma_N$ of −160 ppm (28) were determined. Independently, solution NMR experiments yielded values for $\Delta\sigma_H$ of backbone amide protons in the range 3 to 15 ppm (37) and $\Delta\sigma_N$ near −170 ppm (10).

Discussion

In the experiments with the *ftz* homeodomain-DNA complex the overall transverse relaxation rates of ^{15}N and $^{1}H^{N}$ in the

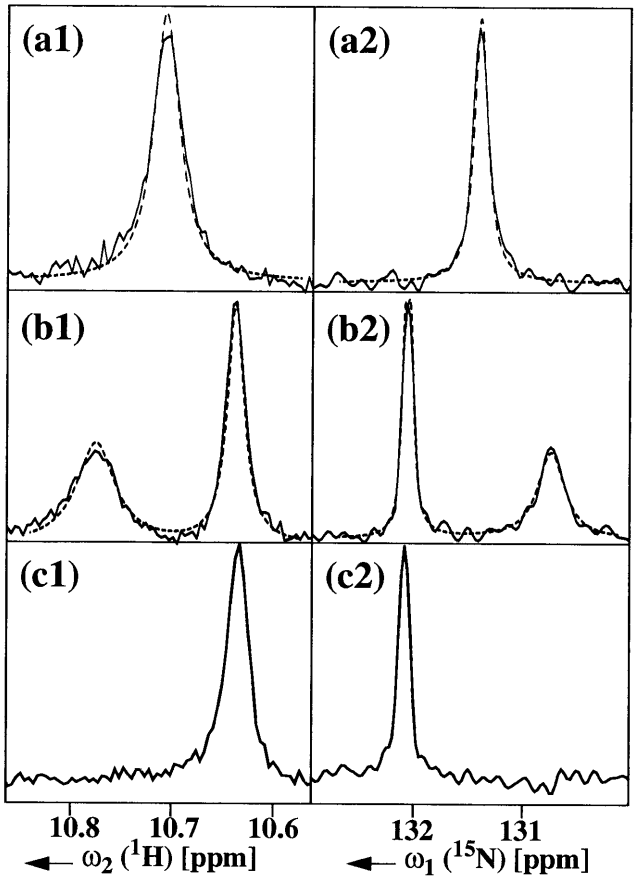

FIG. 3. Cross-sections through the spectra of Fig. 2 (solid lines). To facilitate a comparison of the linewidths in the different spectra the cross-sections were normalized to the same maximal signal amplitude. (*a1*), (*a2*), etc. refer to the arrows in Fig. 2. Simulated line shapes (dashed lines in *a* and *b*) were calculated using $^1J(^1H,^{15}N) = -105$ Hz, a rotational correlation time of $\tau_c = 20$ ns, and chemical shift anisotropies of $\Delta\sigma_H = -16$ ppm and $\Delta\sigma_N = -160$ ppm. A long-range scalar coupling $^2J(^1H^{\delta1},^{15}N^{\varepsilon1}) = -5$ Hz was included in the simulation of the ^{15}N lineshapes (24), but possible effects of the small scalar couplings $^3J(^1H^{\delta1},^1H^{\varepsilon1})$ and $^3J(^1H^{\zeta2},^{15}N^{\varepsilon1})$ were neglected. For $^1H^N$ the relaxation due to DD coupling with other protons in the nondeuterated complex was approximated by three protons placed at a distance of 0.24 nm from $^1H^N$.

indole ^{15}N–^1H moiety of a buried tryptophan were reduced by 60% and 40%, respectively, when using a TROSY-type [^{15}N,^1H]correlation experiment instead of the conventional [^{15}N,^1H]COSY scheme. At a first glance this may appear to be a modest improvement, but a closer look reveals that DD coupling with remote protons, which could be nearly completely suppressed by replacement of the nonlabile hydrogen atoms with ^2H (e.g., refs. 6 and 8), accounts for 95% of the residual $T_2(^1H^N)$ relaxation and 75% of the residual $T_2(^{15}N)$ relaxation. In a corresponding DNA complex with the perdeuterated *ftz* homeodomain the reduction of the T_2 relaxation rates of the ^{15}N–^1H moieties by the use of TROSY at 750 MHz would be about 40-fold for $^1H^N$ and about 10-fold for ^{15}N.

Using Eqs. **1–6** with $\Delta\sigma_H = -16$ ppm, $\Delta\sigma_N = -160$ ppm, $\mathbf{r}_{HN} = 0.101$ nm and parallel orientation of the principal axis of the CSA tensor with the vector $\mathbf{r}_{HN}$, we evaluated the dependence of the residual T_2 relaxation rates of ^{15}N and ^1H in TROSY-type experiments on the polarizing magnetic field B_0 and the molecular size. These calculations showed that nearly complete compensation of T_2 relaxation because of DD and CSA within the ^{15}N–^1H moieties is obtained at a B_0 strength corresponding to a ^1H frequency near 1,100 MHz, i.e., at this field strength $(p - \delta_S) \cong 0$ and $(p - \delta_I) \cong 0$ in Eq. **2**. Theory further predicts that the residual TROSY T_2 relaxation rates because of DD and CSA interactions within the ^{15}N–^1H fragment are practically independent of the molecular size. For perdeuterated proteins the size limit for TROSY-type [^{15}N,^1H]correlation experiments thus is not critically determined by T_2 relaxation, but one needs nonetheless to consider that the effect of deuteration of the nonlabile proton sites in the protein is dependent on conformation. For the ^{15}N–^1H moieties in β-sheet secondary structure, DD and CSA interactions within the ^{15}N–$^1H^N$ fragment are the only sources of transverse relaxation that need to be considered, whereas in α-helices the two sequentially adjacent $^1H^N$ protons (3) contribute significantly to the transverse relaxation of the ^{15}N and $^1H^N$ spins.

To provide a tangible illustration (Fig. 4) we calculated the $^1H^N$ and ^{15}N line shapes for two perdeuterated spherical proteins in ^1H_2O solution with rotational correlation times τ_c of 60 and 320 ns, which corresponds to molecular masses of 150 and 800 kDa, respectively. A magnetic field B_0 corresponding to a resonance frequency 750 MHz for protons was assumed. To account for the worst possible situation for DD interaction with remote protons, two protons were placed at 0.29 nm from $^1H^N$. The linewidth of the narrow component of the ^{15}N doublet increases only slightly with molecular mass and is about 5 Hz at 150 kDa and 15 Hz for a 800-kDa protein (Fig. 4). The $^1H^N$ linewidth depends more strongly on the residual DD interactions with remote protons and is about 15 Hz at 150 kDa and 50 Hz for a 800-kDa protein. For the 150-kDa protein these numbers correspond to 10- and 4-fold reduction of the ^{15}N and $^1H^N$ TROSY linewidths, respectively, when compared with a conventional [^{15}N,^1H]COSY experiment with broadband decoupling of ^{15}N and ^1H. For large molecular sizes the experimental scheme of Fig. 1 may, in principle, be further improved by elimination of the 180° refocusing radio frequency

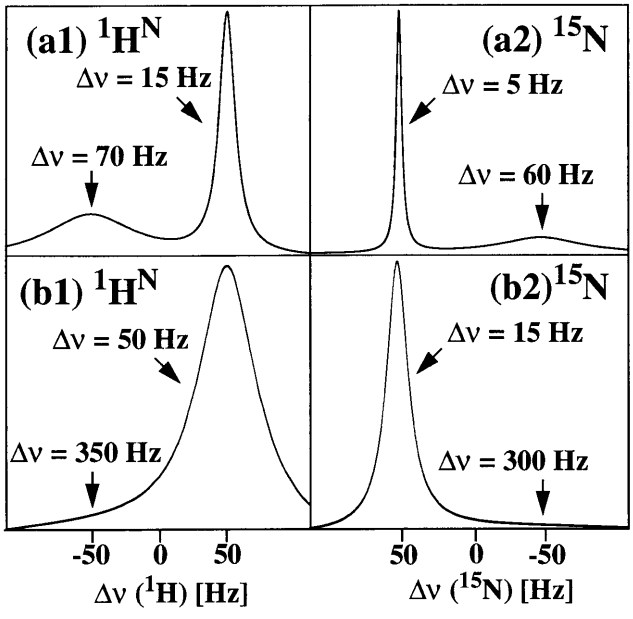

FIG. 4. 1H and ^{15}N lineshapes predicted for the broad and narrow multiplet components of $^1H^N$ and ^{15}N of the ^{15}N–^1H moiety in a [^{15}N,^1H]COSY experiment of the type of Fig. 3 *b*1 and *b*2 for large proteins in H_2O solution at 20°C and a ^1H frequency of 750 MHz. (*a1* and *a2*) Spherical protein of size 150 kDa. For the calculation a rotational correlation time of 60 ns, $\Delta\sigma_H = -16$ ppm and $\Delta\sigma_N = -160$ ppm were used, and all nonlabile protons were replaced with deuterons. Relaxation due to DD coupling with other labile protons was modeled by placing two protons at a distance of 0.29 nm from $^1H^N$. The full linewidths at half height are indicated. (*b1* and *b2*) Spherical protein of size 800 kDa. The calculation used $\tau_c = 320$ ns and otherwise the same parameters as in *a*.

(rf)-pulses during the insensitive nuclei enhanced by polarization transfers (INEPTs), because during the INEPT mixing times these pulses mix the multiplet components with slow and fast T_2 relaxation in a similar way as during the entire experiment in conventional [^{15}N,^{1}H]COSY. The elimination of decoupling sequences and 180° pulses from TROSY-type NMR pulse sequences also may have implications for future probe designs, because the constraints by the requirements for minimal radio frequency heating and maximal B_1 homogeneity then may be relaxed, permitting a better optimization of other parameters such as sensitivity or sample diameter.

The TROSY principle drastically reduces all major sources of relaxation throughout the entire NMR experiment, including signal acquisition, and is clearly distinct from the use of heteronuclear multiple-quantum coherence to reduce dipolar relaxation between heteronuclei (29), which previously was used for measurements of $^{3}J_{H\alpha H\beta}$ scalar coupling constants in proteins (30). Heteronuclear multiple-quantum coherences are subject to dipolar relaxation with remote spins as well as to CSA relaxation, which limits the use of these coherences at high polarizing magnetic fields. Moreover, the slow relaxation of the multiple-quantum coherences cannot be used during signal acquisition (14), which is critical for large molecules.

The following are some initial considerations on practical applications of the TROSY principle: (*i*) Because only one of the four multiplet components of ^{15}N–^{1}H moiety is retained in TROSY-type experiments, the conventional [^{15}N,^{1}H]COSY is intrinsically more sensitive. However, for measurements with proteins at ^{1}H frequencies higher than 500 MHz, TROSY will provide a much better ratio of signal height to noise. (*ii*) TROSY-type [^{13}C,^{1}H]correlation experiments with the ^{13}C–^{1}H moieties of the aromatic rings of Tyr, Phe, and Trp yield comparable results to those for ^{15}N–^{1}H moieties (unpublished results). (*iii*) Two-dimensional nuclear Overhauser effect spectroscopy (NOESY) experiments correlating amide protons and aromatic protons can be relayed by TROSY-type heteronuclear correlation experiments. In favorable cases this might result in low resolution structures for several-fold larger proteins than have been accessible so far. (*iv*) We anticipate that a wide variety of NMR experiments currently used for resonance assignments and collection of conformational constraints can be optimized for larger molecular sizes by use of the TROSY approach in one or several dimensions.

Appendix: Quantitative Analysis of TROSY

The coherence transfer during the pulse sequence of Fig. 1 was evaluated using the product operator formalism (31) as implemented in the program POMA (32), and the resulting phases of the rf-pulses and the receiver were transferred into the experimental pulse program according to (33). The transverse proton magnetization after the first 90° pulse on protons (*a* in Fig. 1) then is given by Eq. **8**:

$$\sigma(\mathbf{a}) = -I_y. \qquad [8]$$

During the delay $2\tau_1$ the scalar coupling $^{1}J(^{1}\mathrm{H},^{15}\mathrm{N})$ evolves, so that the first 90°(^{15}N) pulse generates two-spin coherence. With $\tau_1 = 1/(4^{1}J(^{1}\mathrm{H},^{15}\mathrm{N}))$ we have at time **b** for the first step of the phase cycle (Fig. 1):

$$\sigma_1(\mathbf{b}) = 2I_zS_x = I_zS^- + I_zS^+ \quad (\Psi_1 = y). \qquad [9]$$

The evolution of these terms during t_1, including relaxation, was evaluated using the single-transition basis operators $S^{\pm}_{12}$ and $S^{\pm}_{34}$:

$$S^{\pm}_{12} = \tfrac{1}{2}S^{\pm} + I_zS^{\pm}, \qquad [10]$$

$$S^{\pm}_{34} = \tfrac{1}{2}S^{\pm} - I_zS^{\pm}. \qquad [11]$$

The time evolution of the expectation values of these operators can be obtained by integration of Eq. **1** with initial conditions derived from Eq. **9** and the assumption that $1/T_{1I} \ll {}^{1}J(^{1}\mathrm{H},^{15}\mathrm{N})$, which results in the following density matrix at time **c**:

$$\begin{aligned}\sigma_1(\mathbf{c}) = {} & \frac{1}{2}S^-(\exp[i\omega_S^{12}t_1 - R_{12}t_1] - \exp[i\omega_S^{34}t_1 - R_{34}t_1]) \\ & + I_zS^-(\exp[i\omega_S^{12}t_1 - R_{12}t_1] + \exp[i\omega_S^{34}t_1 - R_{34}t_1]) \\ & + \frac{1}{2}S^+(\exp[-i\omega_S^{12}t_1 - R_{12}t_1] - \exp[-i\omega_S^{34}t_1 \\ & - R_{34}t_1]) + I_zS^+(\exp[-i\omega_S^{12}t_1 - R_{12}t_1] \\ & + \exp[-i\omega_S^{34}t_1 - R_{34}t_1]). \qquad [12]\end{aligned}$$

The relaxation factors R_{ij} are related to the individual relaxation rates of the multiplet components by Eqs. **13** and **14**:

$$R_{jk} = R_{jkjk} + 1/T_{2S} + 1/(2T_{1I}) \quad (jk = 12, 34), \qquad [13]$$

$$R_{jk} = R_{jkjk} + 1/T_{2I} + 1/(2T_{1S}) \quad (jk = 13, 24). \qquad [14]$$

The subsequent polarization transfer step (time period **c** to **d** in Fig. 1) links the evolution period t_1 with the acquisition period t_2. The density matrix at time point **c** is represented by Eq. **15**, where only those I^- and I^-S_z coherences are retained that result in detectable signals during data acquisition:

$$\begin{aligned}\sigma_1(\mathbf{d}) = {} & \frac{1}{2}I^-(i\cos[\omega_S^{12}t_1] - \sin[\omega_S^{12}t_1])\exp[-R_{12}t_1] \\ & + \frac{1}{2}I^-(i\cos[\omega_S^{34}t_1] + \sin[\omega_S^{34}t_1])\exp[-R_{34}t_1] \\ & - I^-S_z(i\cos[\omega_S^{12}t_1] - \sin[\omega_S^{12}t_1])\exp[-R_{12}t_1] \\ & + I^-S_z(i\cos[\omega_S^{34}t_1] + \sin[\omega_S^{34}t_1])\exp[-R_{34}t_1]. \qquad [15]\end{aligned}$$

The other steps in the phase cycle of Fig. 1 can be analyzed in an analogous fashion. Accumulation of the eight transients of the pulse sequence results in the following density matrix for the real part of the interferogram:

$$\begin{aligned}\sigma_{Re}(\mathbf{d}) = {} & -4I^-\sin[\omega_S^{12}t_1]\exp[-R_{12}t_1] \\ & + 8I^-S_z\sin[\omega_S^{12}t_1]\exp[-R_{12}t_1]. \qquad [16]\end{aligned}$$

Incrementation of the phase ψ_1 by 90° at each discrete value of t_1 leads to the corresponding imaginary part:

$$\begin{aligned}\sigma_{Im}(\mathbf{d}) = {} & -4I^-\cos[\omega_S^{12}t_1]\exp[-R_{12}t_1] \\ & + 8I^-S_z\cos[\omega_S^{12}t_1]\exp[-R_{12}t_1]. \qquad [17]\end{aligned}$$

Eqs. **16** and **17** are combined to the hypercomplex interferogram that represents pure phase correlation in the ω_1 dimension.

The treatment of the relaxation of the $^{1}H^{N}$ coherences during the acquisition period t_2 is similar to the treatment of ^{15}N during t_1 (see *Theory*). The signals generated by I^- and I^-S_z coherences that are received during t_2 are described by Eqs. **18** and **19**, respectively:

$$I^- \rightarrow A(\exp[i\omega_I^{13}t_2 - R_{13}t_2] + \exp[i\omega_I^{24}t_2 - R_{24}t_2]) \qquad [18]$$

$$2I^-S_z \rightarrow A(\exp[i\omega_I^{13}t_2 - R_{13}t_2] - \exp[i\omega_I^{24}t_2 - R_{24}t_2]), \qquad [19]$$

where A is a proportionality coefficient. Substitution of Eqs. **18** and **19** into Eqs. **16** and **17** results in the hypercomplex

interferogram corresponding to the 1→2 and 2→4 transitions of the $^1H,^{15}N$ spin system:

$$\sigma_{1224} = 8A\exp[i\omega_S^{12}t_1 + i\omega_I^{24}t_2]\exp[-(R_{12}t_1 + R_{24}t_2)]. \quad \textbf{[20]}$$

Finally, the Fourier transformation of the hypercomplex interferogram represented by Eq. **20** results in the pure absorptive correlation spectrum, with resonance frequencies in ω_1 and ω_2 corresponding to the desired individual component of the ^{15}N–^1H multiplet.

We thank M. Wahl for the preparation of the *ftz* homeodomain-DNA complex and Dr. R. Brüschweiler for critical reading of the manuscript. Financial support was obtained from the Schweizerischer Nationalfonds (Project 31.49047.96).

1. Shulman, R. G., Ogawa, S., Wüthrich, K., Yamane, T., Peisach, J. & Blumberg, W. E. (1969) *Science* **165,** 251–257.
2. Arata, Y., Kato, K., Takahashi, H. & Shimada, I. (1994) *Methods Enzymol.* **239,** 440–464.
3. Wüthrich, K. (1986) *NMR of Proteins and Nucleic Acids* (Wiley, New York).
4. Wüthrich, K. (1995) *NMR in Structural Biology* (World Scientific, Singapore).
5. Wüthrich, K. (1995) *Acta Cryst. D* **51,** 249–270.
6. Shan, X., Gardner, K. H., Muhandiram, D. R., Rao, N. S., Arrowsmith, C. H. & Kay, L. E. (1996) *J. Am. Chem. Soc.* **118,** 6570–6579.
7. Wagner, G. (1993) *J. Biomol. NMR* **3,** 375–385.
8. Nietlispach, D., Clowes, R. T., Broadhurst, R. W., Ito, Y., Keeler, J., Kelly, M., Ashurst, J., Oschkinat, H., Domaille, P. J. & Laue, E. D. (1996) *J. Am. Chem. Soc.* **118,** 407–415.
9. Guéron, M., Leroy, J. L. & Griffey, R. H. (1983) *J. Am. Chem. Soc.* **105,** 7262–7266.
10. Tjandra, N., Szabo, A. & Bax, A. (1996) *J. Am. Chem. Soc.* **118,** 6986–6991.
11. Farrar, T. C. & Stringfellow, T. C. (1996) in *Encyclopedia of NMR*, eds. Grant, D. M. & Harris, R. K. (Wiley, New York), Vol. 6, pp. 4101–4107.
12. Vold, R. R. & Vold, R. L. (1978) *Prog. NMR Spectrosc.* **12,** 79–133.
13. Ernst, R. R., Bodenhausen, G. & Wokaun, A. (1987) *The Principles of Nuclear Magnetic Resonance in One and Two Dimensions* (Clarendon, Oxford).
14. Abragam, A. (1961) *The Principles of Nuclear Magnetism* (Clarendon, Oxford).
15. Goldman, M. (1984) *J. Magn. Reson.* **60,** 437–452.
16. London, R. E. (1990) *J. Magn. Reson.* **86,** 410–415.
17. Peng, J. W. & Wagner, G. (1992) *J. Magn. Reson.* **98,** 308–332.
18. Percival-Smith, A., Müller, M., Affolter, M. & Gehring, W. J. (1990) *EMBO J.* **9,** 3967–3974.
19. Qian, Y. Q., Furukubo-Tokunaga, K., Resendez-Perez, D., Müller, M., Gehring, W. J. & Wüthrich K. (1994) *J. Mol. Biol.* **238,** 333–345.
20. Kay, L. E., Torchia, D. A. & Bax, A. (1989) *Biochemistry* **28,** 8972–8979.
21. Farrow, N. A., Muhandiram, R., Singer, A. U., Pascal, S. M., Kay, C. M., Gish, G., Shoelson, S. E., Pawson, T., Forman-Kay, J. D. & Kay, L. E. (1994) *Biochemistry* **33,** 5984–6003.
22. Müller, L, (1979) *J. Am. Chem. Soc.* **101,** 4481–4484.
23. Bodenhausen, G. & Ruben, D. J. (1980) *Chem. Phys. Lett.* **69,** 185–189.
24. Bystrov, V. F. (1976) *Prog. NMR Spectrosc.* **10,** 41–81.
25. Palmer, A. G., Skelton, N. J., Chazin, W. J., Wright, P. E. & Rance, M. (1992) *Mol. Phys.* **75**, 699–711.
26. Kay, L. E., Nicholson, L. K., Delaglio, F., Bax, A. & Torchia, D. A. (1992) *J. Magn. Reson.* **97**, 359–375.
27. Michal, C. A., Wehman, J. C. & Jelinski, L. W. (1996) *J. Magn. Reson. Ser. B.* **111,** 31–39.
28. Hiyama, Y., Niu, C., Silverton, J. V., Bavoso, A. & Torchia, D. A. (1988) *J. Am. Chem. Soc.* **110**, 2378–2383.
29. Griffey, R. H. & Redfield, A. G. (1987) *Quart. Rev. Biophys.* **19,** 51–82.
30. Grzesiek, S., Kuboniwa, H., Hinck, A. P. & Bax, A. (1995) *J. Am. Chem. Soc.* **117,** 5312–5315.
31. Sørensen, O. W., Eich, G. W., Levitt, M. H., Bodenhausen, G. & Ernst R. R. (1983) *Prog. NMR Spectrosc.* **16,** 163–192.
32. Güntert, P., Schaefer, N., Otting, G. & Wüthrich, K. (1993) *J. Magn. Reson.* **101,** 103–105.
33. Levitt, M. H. (1997) *J. Magn. Reson.* **126,** 164–182.
34. Piotto, M., Saudek, V. & Sklenar, V. J. (1992) *J. Biomol. NMR* **2,** 661–665.
35. McConnell, H. M. (1956) *J. Chem. Phys.* **25,** 709–715.
36. Shimizu, H. (1964) *J. Chem. Phys.* **40,** 3357–3364.
37. Tjandra, N. & Bax, A. (1997) *J. Am. Chem. Soc.* **119,** 8076–8082.